A Detailed Full-Cell Model of a 2018 Commercial PERC Solar Cell in Quokka3

Andreas Fell, Pietro P. Altermatt

***Abstract*— An unprecedented detailed model of a full-size PERC solar cell design, as manufactured at a current Trina Solar production-line during ramp-up, is presented. Combining a newly proposed multidomain approach with the multiscale skin-concept of Quokka3, the 15.6 cm x 15.6 cm 3D cell geometry including the details of the emitter skins can thoroughly be solved within a single simulation. The multidomain approach uses an inner and two edge domains as irreducible symmetry elements, each containing the unequal front and rear pitch, the dashed rear contacts, as well as part of the busbars and consequently the full finger resistance. The full-cell current density is then determined by simple area-averaging, opposed to the more complicated common approach of coupling it with a distributed network model. The multiscale skin approach enables to model all emitter parts of the PERC cell in detail (accounting for dopant profiles, front surface recombination, Fermi-Dirac statistics etc.), whereas the other skin regions can still be described by their lumped properties, i.e. R_{sheet} and J_0 / S_{eff}. A complete set of carefully established electrical and optical input parameters as well as a detailed loss breakdown is presented, providing fellow researchers with a point of reference for modeling a state-of-the-art PERC solar cell in 2018.**

***Index Terms*—Modeling, solar cell, PERC, Quokka, simulation, silicon, PERC, full-cell**

I. Introduction

The ultimate way to simulate a silicon solar cell would be to solve the well-established semiconductor differential equations for the full-size 3D geometry. However, this would presently require a computer cluster and many hours [1]. Therefore, the common approach to model solar cells is to solve the semiconductor differential equations within a small "unit cell" domain. Large scale effects, such as metal grid resistance, busbar shading, and edge recombination, are not covered in such a domain. The most accurate approximation to include full-size effects has been to connect such unit cell simulations within a SPICE model, an approach applied already in the 1970's [2] and later e.g. in [3, 4]. The SPICE model is fed with the IV curves of possibly various different "unit cell" domains from the inner and the edge part of the cell. Other ways of including large scale effects are simplifications to e.g. a lumped series resistance, scaling of the current density, and an external diode property. Often, at least some of these large-scale effects are even neglected. These simplifications reduce the level of detail and accuracy, and thus the predictive power of the simulations. A notable exception exists with Griddler [5], which rigorously solves a distributed diode network representing a full-size solar cell including its metallization, at the expense of lumping multidimensional semiconductor transport effects into quasi-1D two-diode circuits.

Recently, Quokka3 was presented to be capable of discretizing and electrically solving an entire full cell geometry in 3D including the metal layers. This became possible by the "skin concept", where the near-surface regions are treated as lumped boundary conditions to the quasi-neutral bulk carrier transport, omitting the fine discretization required within a full detailed model [6, 7]. The lumped skins are characterized mainly by their sheet resistance R_{sheet} and recombination property $J_{0,skin}$. Yet, Quokka3 can still account for the detailed physics of a skin by employing a "multiscale" approach, where the semiconductor differential equations are solved in 1D within the skin and are consistently coupled as an extended boundary condition to the 3D bulk solver [6]. It is therefore now practically possible to accurately solve full-size geometries with low complexity in 3D (like 156 mm Al-BSF cells), including detailed skin properties, i.e. equivalent to a full detailed cell model. However, computational demand is substantial, and still prohibitively high on standard hardware for more complex geometries, e.g. PERC cells with dashed rear contacts or IBC cells.

This work presents a "multidomain" approach (originally introduced in [8]) to enhance the capabilities for full-cell modeling of Quokka3 further: three (or if necessary more) domains can be combined for modeling a front and rear contacted cell with H-pattern metallization. This enables solving e.g. a full-size PERC solar cell with dashed rear-contacts and unequal front and rear contact pitches in practical computing times (<hours). In this way, a wide range of effects relevant for PERC cells can be modelled within a single simulation domain: from the details of the emitter skin losses (e.g. Auger and surface recombination), over medium-scale effects (e.g. 3D spreading resistance effects at the local rear dash contacts), up to full cell effects (e.g. edge effects).

The new capabilities are showcased on a recent production-line Trina PERC cell. The input parameters are derived by

Andreas Fell acknowledges financial support by the European Commission through the Marie-Curie fellowship "Quokka Maturation".

A. Fell is with the Fraunhofer Institute for Solar Energy Systems, 79110 Freiburg, Germany (e-mail: andreas.fell@ise.fraunhofer.de).

P.P. Altermatt is with Trina Solar, State Key Laboratory of PV Science and Technology, Changzhou, Jiangsu Province, 213031 China (e-mail: pietro.altermatt@trinasolar.com).

A. Fell is also with AF simulations, 79232 March, Germany (email: andreas@quokka3.com)

independent measurements on test-structures, and carefully calibrated against the final cell characteristics. Details of how to establish the lumped-parameter optical model of Quokka3, a detailed loss breakdown, and the complete set of (lumped) input parameters are given.

II. Multidomain full-cell model

The multidomain approach of this work can be considered an extreme case of the unit-cell simulations + SPICE approach described in the introduction. Enabled by the performance of Quokka3, much larger domains compared to the common unit cell domain can be used. Most decisively, the domains span over half a busbar-pitch, thus fully including the current-transport through the metal fingers and its accompanying potential drop, as well as busbar recombination and shading. Furthermore, it gives more freedom for different front and rear contact pitches, using the least-common-multiplier to derive the total domain width. This is in contrast to common unit cell simulations, where almost always the pitches are adjusted to 1/1, 1/2 (and rarely 3/4) ratios. In this case, 3.5 front metal fingers (105 total) and 6.5 lines of rear dashed contacts (195 total) define the width of the domains.

The three large domains comprise an inner domain (domain 0) and two edge domains: perpendicular to the fingers with or without a redundant line (domain 1), and parallel to the fingers (domain 2), see Fig. 1 and Fig. 2. Using the well justified assumption that the busbar has a constant potential which equals the applied potential, i.e. neglecting busbar resistance, the electrical network simplifies to the summation of the currents from the areas represented by the respective domains at a given applied voltage. For ease-of-use and overall consistency, Quokka3 can automatically construct the domains from the user-defined full cell geometry with a H-pattern metallization and internally perform the current summation. Therefore, the inputs are the same as defining the full-cell geometry, with simply an additional option whether to use the multidomain approach. This enables a straightforward variation of all input parameters including the geometry, with the decisive benefit of computational demand being reduced to a practical level compared to solving the actual full-size domain.

Note that an approximation implied by the multidomain model is that the four corners of the cell are represented by two adjacent edge domains, which however incurs very small errors [3].

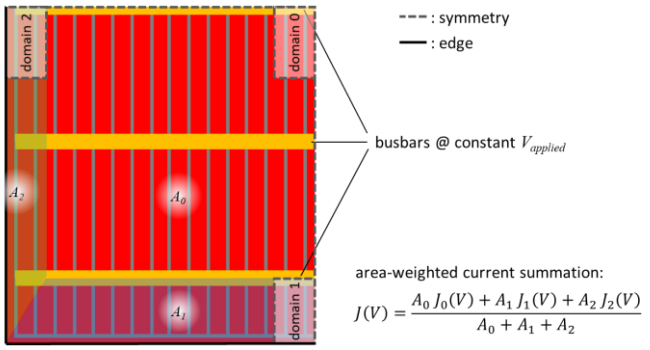

Fig. 1. Sketch of a H-pattern 5 busbar cell design (quarter symmetry, not to scale), showing the 3 domains of the multidomain approach.

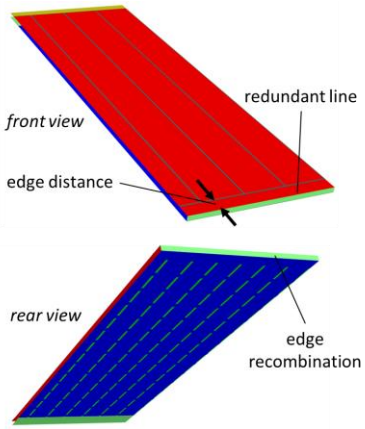

Fig. 2. Detailed view of edge domain 1 for the investigated PERC cell, highlighting the different front and rear contact pitch, the dashed rear contacts, and the inclusion of the finger resistance.

III. Application example: industrial PERC cell

A. Electrical and optical cell properties

The multidomain approach is applied to a production-line Trina Solar cell during ramp-up. The efficiency is only close to 21% because it was fabricated during ramp-up, and therefore this cell does not represent the cells sold by Trina, but enabling us to disclose more details. The various input parameters required for the simulations were carefully derived from dedicated test structures, see Table A in the Appendix for a summary. Our simulations simultaneously match the manufactured cell IV parameters, the reflection and external quantum efficiency closely, see Table I and Fig. 3, meaning that a highly predictive model is achieved. We note that thereby this work provides a complete (lumped) input parameter set describing a (close-to) state-of-the-art industrial PERC cell in 2018. This is to our knowledge the best available parameter set to date to describe a recent commercial PERC cell, and thus provides an update to the 2014 PERC model published in [9].

Table I
Comparison of experimental (median over 2000 cells) and (baseline) simulated IV parameters of a Trina PERC cell during ramp up, hence not fully representing commercial cells.

	V_{oc} [mV]	J_{sc} [mA/cm²]	FF [%]	η [%]
experimental	667	39.4	80.5	21.2
simulation	669	39.4	80.6	21.2

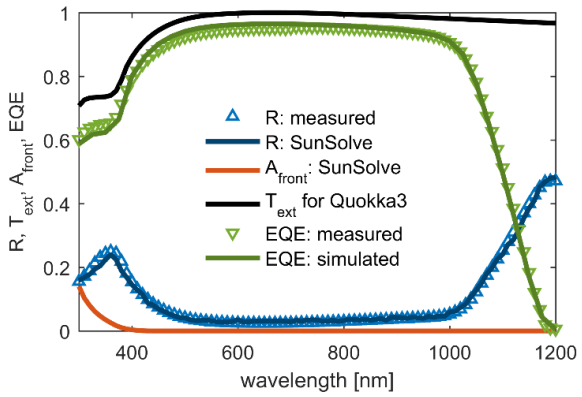

Fig. 3. SunSolve fitted to measured reflection *R*, the resulting simulated front film absorption A_{front}, the derived T_{ext}, and EQE comparison between measurement and Quokka3 simulation.

To derive the generation rate, Quokka3's T_{ext}-Z optical model is used [10]. Fitting well in scope with the skin concept, the inputs for this model are lumped optical parameters of the cell, mainly the transmission through the front surface T_{ext}, and light trapping quantified via the path-length enhancement factor Z. In this work we choose to input internal optical properties of the various skins, from which Quokka3 internally calculates Z for each combination of front and rear skins using the analytical model of Brendel et al. [11]. Most notably, this enables us to account for the spatially varying light trapping performance of the device due to the different internal reflectivity of the different rear regions: i) the poorly reflecting localized contacts, ii) the well reflecting passivated area covered by Al-paste, and iii) the even higher reflecting Ag-paste area. In this way, we increase the predictive power of the model as it can consider the changes in current for varying rear cell design in addition to shading from the front metal grid. In contrast to using a static generation profile, the T_{ext}-Z model further comes with the benefits of supporting quantum efficiency simulations, thickness variation and even temperature variation within Quokka3 using a fixed set of optical input parameters [10].

To derive T_{ext} and the internal optical properties of the skins, we setup detailed optical simulations of the three different cell areas in the optical simulator SunSolve from PV lighthouse [12, 13], being careful in replicating the measured reflection of the cells under investigation.

T_{ext} is then determined by one minus the measured reflectance (corrected to exclude metal), linearly extrapolating in the long wavelengths to exclude the escape reflection, and adding the front film absorption from the SunSolve results for the short wavelengths.

The SunSolve results further contain the light trapping performance of the device which can be quantified by the path-length enhancements factor Z. In a subsequent step we find the lumped internal optical properties by fitting the analytical model [11] implemented in Quokka3 to match the known Z, see Fig. 4. In the analytical model we first fix the internal front reflectance to an average reflectance of 0.93 and a specular reflectance of 0.62, as proposed in [11] for a typical random-pyramid textured surface with anti-reflection coating. Agreement with the SunSolve results is achieved with a physically meaningful trend of the average rear reflectance between the different regions, as well as their Lambertian fraction: the contacted Al-BSF areas have a relatively low reflectance but high scattering, whereas the Al- and Ag-covered passivated areas scatter less but have a higher reflectance, see Fig. 4. Employing those values within the complete cell simulation overestimates J_{sc} by only ~0.3 mA/cm². Possible reasons are neglecting the effect of parasitic internal absorption at the front contacts and free carrier absorption in the heavily doped areas. However, both reduce the light trapping performance only slightly [14]. We therefore adjust the average internal front reflectance down to 0.85 to match the experimental J_{sc}. This value is similar to the value evaluated in UNSW PERL cells in staggered pyramids [15] and may well be realistic for the random textures of mass-fabricated PERC cells. In Fig. 3 a comparison between the final simulated and measured external quantum efficiency (EQE) is shown, which shows very good agreement for all wavelengths and thus validates the optical model established for this cell.

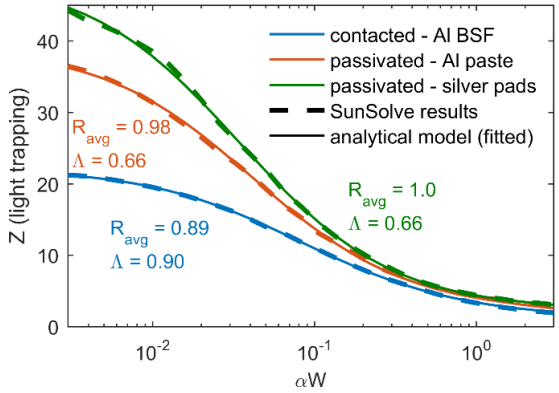

Fig. 4. Light trapping quantified by Z comparing SunSolve results with the analytical model used in Quokka3.

The non-contacted part of the emitter skins, i.e. the n+ as well as the non-contacted n++ emitter regions, are modelled using the experimentally measured doping profiles and the silicon recombination properties given in Ref. [1]. Modelling the non-contacted emitter regions in detail is useful for a detailed loss analysis, and in this case also for considering the significant current collection losses in the 300 µm wide n++ emitter regions which are rather wide to ensure alignment with the screen-printing metallization. It is sensible to model the contacted skins (contacted part of the emitter and the rear local BSFs) as well as the rear-passivation using lumped parameters ($J_{0,skin}$ and R_{sheet}). This is due to substantially larger uncertainties of the detailed inputs and highlights the flexibility of Quokka3's multiscale modelling approach, which allows to individually set the modelling type of the different skins. We note that the actual volumetric shape of the local rear contacts have to be simplified to a planar rectangular area due to the cuboidal mesh type in Quokka3. Any deviation arising from that simplification can be considered to be effectively "lumped" into the $J_{0,skin}$ of the rear contacts.

We model edge losses for two extreme cases of no and "worst-case" edge recombination. Worst-case means assuming edge SRV's at thermal velocity, accounting for both the edge of the quasi-neutral bulk region, as well as within the space-

charge-region as a result of the emitter reaching to the edge. For the "baseline" input parameters which are compared to experimental results we assume no edge recombination, as some degree of passivation is expected during cell processing which likely renders edge recombination losses insignificant. For the loss breakdown in section III.B we assume worst-case edge recombination instead, for the sake of illustrating the large range of losses being accessible via a single simulation. The reader is referred to [16] for details on the assumptions and the implementation of edge recombination in Quokka3, and to [8] for an edge loss study of the investigated PERC cell.

B. Loss Breakdown

Finally, we present a power loss breakdown of the investigated PERC cell. The breakdown is based on the free energy loss analysis (FELA) [17] which is an automatic output of Quokka3. The FELA is extended with approximate optical power losses by multiplying the respective current density loss with the maximum power point voltage. Here we choose the worst-case edge recombination scenario to illustrate the convenience of the multi-domain approach to additionally determine the edge power losses: it is directly computed by comparing the total terminal power density with the one from the inner, i.e. edge-effect-free, domain. Within an actual full cell simulation in contrast, the quantification of edge losses is not straightforward, because a suitable edge-effect-free reference simulation would need to be established in addition.

In Fig. 5 the loss breakdown is plotted, highlighting the unprecedented scale of detail achieved within a single simulation. It ranges from large scale effects like edge losses, to resolving the losses within the emitters by Quokka3's multiscale approach. In overall the cell is well balanced, with no single loss channel being obvious to have the dominating potential for improvement.

Regarding optics, shading is the dominant loss followed by escape of light at the front, but which is smaller in the module due to total internal reflection.

On the electrical side, the bulk losses dominate both in terms of recombination via the boron-oxygen (BO) defect SRH recombination and transport losses, making it a candidate for further optimization, e.g. by an improved deactivation of the BO defect and cleaner processing to avoid metal contaminants. The bulk transport losses may be improved by improved cell geometry (smaller pitches), which however requires further simultaneous improvements in finger width and contact recombination to not adversely increase their respective losses. We note further that the losses within the local n++ emitter are not negligible, mainly caused by the large width (300 µm). Thus, an improved alignment technology allowing a smaller width is desirable.

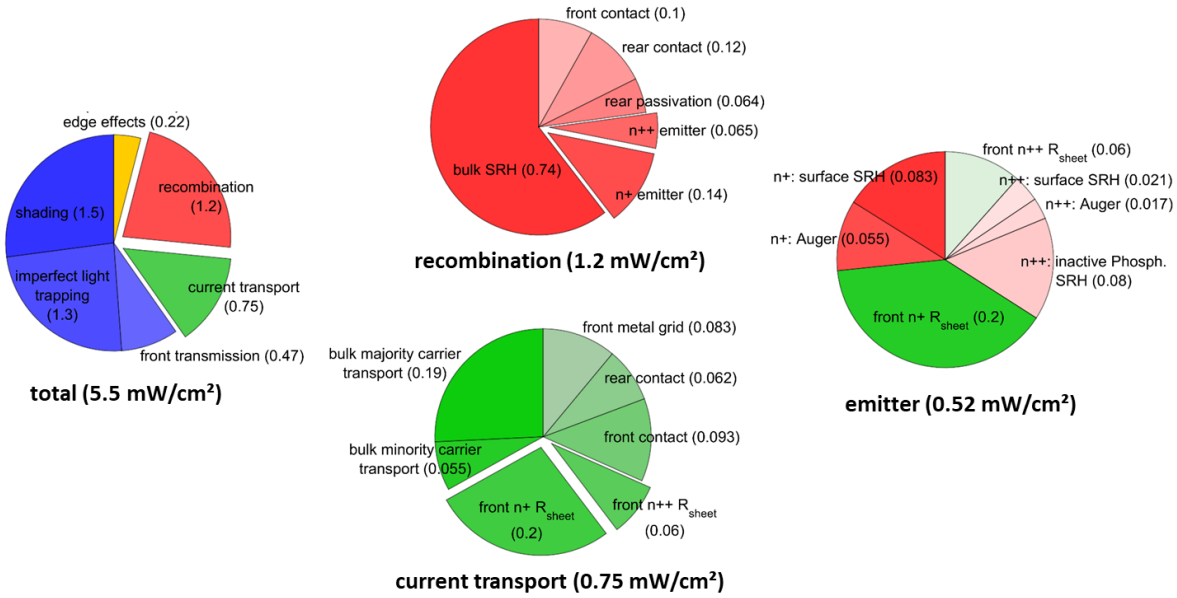

Fig. 5. Detailed power loss breakdown at maximum power point of the investigated PERC cell. Within a single multidomain and multiscale simulation, a wide range of loss details is quantified; note that the results deviate from the baseline model in that worst-case edge recombination [16] is assumed.

IV. Conclusions

The multi-domain approach proposed in this work and implemented in Quokka3 enables to model a full-size PERC cell accounting for a wide range of effects conveniently within a single simulation setup and within practical computing times. While such a range of effects had been possible to model before, it did require multiple software tools and high effort. This work brings such complete cell simulations to a status where it can be routinely included in many modeling tasks.

The approach is showcased on a recent production-line PERC cell of Trina Solar (during ramp-up, not representing commonly fabricated cells) for which a complete and consistent input parameter set is carefully derived to match the experimental cell characteristics. The established PERC model in Quokka3 thus has an unprecedented accuracy and predictive power by a single simulation setup fully accounting for:

- the detailed physics of the emitters, i.e. the interplay of the doping profile with the various recombination mechanisms (Auger, inactive phosphorus SRH and surface SRH), assuming state-of-the-art physical models (Fermi-Dirac carrier statistics, no quasi-neutral assumption, …)
- the actual metal and contact geometry (unequal front and rear contact pitch and dashed rear contacts)
- the accurate distributed resistance effect of the metal grid and the emitter sheet resistance
- 3D carrier transport within the bulk to the localized dashed rear contacts
- busbar effects (localized recombination and shading)
- edge effects (edge geometry, edge recombination)
- wavelength-dependence of the optics, i.e. supporting quantum-efficiency simulations and varying spectral irradiance
- different optical properties of the different rear regions

The careful calibration of electrical and optical properties and overall accuracy of the modelling approach is evidenced by a simultaneous match to the measured reflection, EQE and light JV parameters, giving confidence to its predictive power.

A detailed loss breakdown of the investigated PERC cell is presented, showing that recombination in the base region is dominating the overall recombination losses, but that also recombination within the n++ part of the emitter can be further reduced, and recombination at the metal contacts are significant. It is emphasized, however, that the loss analysis alone is not sufficient for deciding where and how to reduce losses most efficiently; the reduction of losses with design changes must be modeled instead. This is so because large losses are not necessarily easily reduced.

The complete (lumped) input parameter set, given in the appendix, is to our knowledge the best available parameter set to date to describe a commercial PERC cell, which fellow researchers are invited to use as a point of reference.

APPENDIX

TABLE A
ELECTRO-OPTICAL INPUT PARAMETERS FOR THE TRINA SOLAR PRODUCTION-LINE PERC CELL IN AIR (DURING RAMP-UP); A DEVICE TEMPERATURE OF 25°C IS ASSUMED ALONG WITH THE LATEST SI MATERIAL MODELS [1, 9]

general geometry	
cell size	156.75 mm x 156.75 mm
cell thickness	170 µm
distance of metal from cell edge (front and rear)	500 µm
front H-pattern metal grid	
# busbars	5
busbar width	0.8 mm
# fingers	105
finger width	60 µm
optical shading fraction of fingers	0.8
finger sheet resistance	3 mΩ
contact resistivity	2.7 mΩcm²
rear full area metal, dashed contacts	
# busbars (Ag solder pads)	5
busbar width (half of actual 2.2 mm, as the few busbar stripes cover only ~50% of the cell length)	1.1 mm
Al metal sheet resistance	17.5 mΩ
# contact lines	195
# dash contacts per line	155
contact width	72.6 µm
contact length	800 µm
contact resistivity	3 mΩcm²
front n+ skin (*detailed electrical modelling in this work, but disclosing only lumped parameters*)	
sheet resistance	149 Ω
Total J_0	31 fA/cm²
collection efficiency	~1
recombination at exposed pn-junction at edge: $J_{02,edge}$	0 (ideal) / 19 nA/cm (worst case)[16]

T_{ext}	(see Fig. 3)
texture facet angle	53°
average (= diffuse) internal reflectance (effective for contacted and passivated area)	0.85
specular internal front reflectance	0.62
front n++ skin	
(*detailed electrical modelling used in this work for non-contacted part, but disclosing only lumped parameters; optical inputs assumed identical to n+ emitter)*	
width	300 µm
skin depth (required to apply collection efficiency)	0.66 µm
sheet resistance	58 Ω
J_0 non-contacted	120 fA/cm²
J_0 contacted	500 fA/cm²
collection efficiency (at 400 nm)	~0.88
rear skin	
sheet resistance	Inf
S_{eff} non-contacted (both Al- and Ag-covered)	10 cm/s
J_0 contacted	400 fA/cm²
average internal rear reflectance (contacted, Al-, Ag-covered)	0.89, 0.98, 1.0
Lambertian fraction at rear (contacted, Al-, Ag-covered)	0.90, 0.66, 0.66
bulk	
(*BO dominated recombination modelled by single midgap SRH defect*)	
resistivity	1.5 Ωcm
τ_{n0}	150 µs
τ_{p0}	750 µs
recombination at sides (edges): S_{eff}	0 (ideal) / 1×10^7 cm/s (worst case)

V. References

[1] P. P. Altermatt, "Models for numerical device simulations of crystalline silicon solar cells—a review," (English), *J Comput Electron*, vol. 10, no. 3, pp. 314–330, 2011.

[2] C. R. Fang and J. R. Hauser, "A two dimensional analysis of sheet resistance and contact resistance effects in solar cells," in *13th Photovoltaic Specialists Conference*, Washington, 1978, pp. 1306–1311.

[3] G. Heiser, P. P. Altermatt, and J. Litsios, "Combining 2D and 3D device simulation with circuit simulation for optimising high-efficiency silicon solar cells," in *Simulation of Semiconductor Devices and Processes*: Springer, 1995, pp. 348–351.

[4] J. Dicker, J. O. Schumacher, W. Warta, and S. W. Glunz, "Analysis of one-sun monocrystalline rear-contacted silicon solar cells with efficiencies of 22.1%," *J. Appl. Phys.*, vol. 91, no. 7, pp. 4335–4343, 2002.

[5] J. Wong, "Griddler: Intelligent computer aided design of complex solar cell metallization patterns," in *39th Photovoltaic Specialists Conference (PVSC)*, Tampa, FL, USA, 2013, pp. 933–938.

[6] A. Fell, J. Schön, M. C. Schubert, and S. W. Glunz, "The concept of skins for silicon solar cell modeling," *Solar Energy Materials and Solar Cells*, vol. 173, no. Supplement C, pp. 128–133, 2017.

[7] R. Brendel, "Modeling solar cells with the dopant-diffused layers treated as conductive boundaries," *Progress in Photovoltaics: Research and Applications*, vol. 20, no. 1, pp. 31–43, 2012.

[8] A. Fell and P. P. Altermatt, "Detailed 3D Full-Cell Modeling in Quokka3: Quantifying Edge and Solder-Pad Losses in an Industrial PERC Cell," *AIP Journal of Physics*, 2018 (to be published).

[9] A. Fell *et al.*, "Input Parameters for the Simulation of Silicon Solar Cells in 2014," *IEEE Journal of Photovoltaics*, vol. 5, no. 4, pp. 1250–1263, 2015.

[10] A. Fell, K. R. McIntosh, and K. C. Fong, "Simplified Device Simulation of Silicon Solar Cells Using a Lumped Parameter Optical Model," *IEEE J. Photovoltaics*, pp. 1–6, 2016.

[11] R. Brendel, M. Hirsch, R. Plieninger, and J. J.H. Werner, "Quantum efficiency analysis of thin-layer silicon solar cells with back surface fields and optical confinement," *IEEE Transactions on Electron Devices*, vol. 43, no. 7, pp. 1104–1113, 1996.

[12] PV Lighthouse, *SunSolve.* [Online] Available: https://pvlighthouse.com.au/sunsolve. Accessed on: 1st April 2018.

[13] M. D. Abbott, K. R. McIntosh, and B. Sudbury, "Optical loss analysis of pv modules," *EU PVSEC Proceedings*, 2016.

[14] Y. Yang *et al.*, "Combining ray tracing with device modeling to evaluate experiments for an optical analysis of crystalline Si solar cells and modules," *Energy Procedia*, vol. 124, pp. 240–249, 2017.

[15] A. G. Aberle *et al.*, "Limiting loss mechanisms in 23% efficient silicon solar cells," *Journal of Applied Physics*, vol. 77, no. 7, pp. 3491–3504, 1995.

[16] A. Fell *et al.*, "Modeling Edge Recombination in Silicon Solar Cells," *IEEE J. Photovoltaics*, vol. 8, no. 2, pp. 428–434, 2018.

[17] R. Brendel, S. Dreissigacker, N. P. Harder, and P. P. Altermatt, "Theory of analyzing free energy losses in solar cells," *Applied Physics Letters*, vol. 93, no. 17, 173503-173503-3, 2008.